Chemical Science

ROYAL SOCIETY OF CHEMISTRY

EDGE ARTICLE

View Article Online
View Journal | View Issue

Check for updates

Cite this: *Chem. Sci.*, 2019, **10**, 185

All publication charges for this article have been paid for by the Royal Society of Chemistry

Hetero-metallic active sites coupled with strongly reductive polyoxometalate for selective photocatalytic CO_2-to-CH_4 conversion in water†

Shuai-Lei Xie,[a] Jiang Liu,*[b] Long-Zhang Dong,[b] Shun-Li Li,[b] Ya-Qian Lan*[b] and Zhong-Min Su*[ac]

Received 5th August 2018
Accepted 1st October 2018

DOI: 10.1039/c8sc03471k

rsc.li/chemical-science

The photocatalytic reduction of CO_2 to value-added methane (CH_4) has been a promising strategy for sustainable energy development, but it is challenging to trigger this reaction because of its necessary eight-electron transfer process. In this work, an efficient photocatalytic CO_2-to-CH_4 reduction reaction was achieved for the first time in aqueous solution by using two crystalline heterogeneous catalysts, $H\{[Na_2K_4Mn_4(PO_4)(H_2O)_4]\subset\{[Mo_6O_{12}(OH)_3(HPO_4)_3(PO_4)]_4[Mn_6(H_2O)_4]\}\cdot 16H_2O$ (**NENU-605**) and $H\{[Na_6CoMn_3(PO_4)(H_2O)_4]\subset\{[Mo_6O_{12}(OH)_3(HPO_4)_3(PO_4)]_4[Co_{1.5}Mn_{4.5}]\}\cdot 21H_2O$ (**NENU-606**). Both compounds have similar host inorganic polyoxometalate (POM) structures constructed with strong reductive $\{P_4Mo_6^V\}$ units, homo/hetero transition metal ions ($Mn^{II}/Co^{II}Mn^{II}$) and alkali metal ions (K^+ and/or Na^+). It is noted that the $\{P_4Mo_6^V\}$ cluster including the six Mo^V atoms served as a multi-electron donor in the case of a photocatalytic reaction, while the transition metal ions functioned as catalytically active sites for adsorbing and activating CO_2 molecules. Additionally, the presence of alkali metal ions was believed to assist in the capture of more CO_2 for the photocatalytic reaction. The synergistic combination of the above-mentioned components in **NENU-605** and **NENU-606** effectively facilitates the accomplishment of the required eight-electron transfer process for CH_4 evolution. Furthermore, **NENU-606** containing hetero-metallic active sites finally exhibited higher CH_4 generation selectivity (85.5%) than **NENU-605** (76.6%).

Introduction

The massive discharge of CO_2 resulting from the combustion of limited fossil fuels is leading to global warming, which has driven people to find effective ways to alleviate this crisis.[1–4] The photocatalytic reduction of CO_2 to valuable hydrocarbon fuels, such as methane (CH_4), provides a promising 'one stone two birds' approach to realize the purpose of eliminating energy shortage and environmental challenges.[5,6] Nevertheless, the accomplishment of this catalytic reaction means that chemically inert CO_2 molecules adsorbed on the catalyst have to undergo a proton-assisted multi-electron transfer process; it is a rather challenging task for catalyst design because of the uncontrollable multi-electron supply and complicated photocatalytic reaction mechanism.[7,8] Moreover, the heterogeneous nature of the catalyst in principle is also indispensable in view of its practical application.[7,9–17] So far, the studies on heterogeneous catalysts, especially those applied in the photocatalytic reduction of CO_2 to CH_4, mainly focus on nano-sized semiconducting materials or composites[18–21] because of their rich interfacial modification and structural stability that are beneficial for the photocatalytic CO_2 reduction reaction (CO_2RR) towards high activity and good photocatalytic durability.[22–27] It is well-known that these inorganic nanomaterials are stable, but their indistinct active sites and even their electron donors are commonly difficult for the explanation of the photocatalytic reaction mechanism.[28] Also, the introduction of noble metal co-catalysts or heterojunctions sometimes would raise the cost and/or cover the surface active sites to obstruct incident light absorption, which results in reduced photo-conversion efficiency. Consequently, the construction of crystalline inorganic heterogeneous catalysts with well-defined active sites and multi-electron sources would be a better choice for obtaining multi-electron reductive hydrocarbon fuels and investigating the mechanism of the photocatalytic CO_2RR.[29]

Polyoxometalate (POM) with inherent redox and semiconductor features is one kind of inorganic crystalline material,

---

[a] *Institute of Functional Material Chemistry, Department of Chemistry, National & Local United Engineering Lab for Power Battery, Northeast Normal University, Changchun 130024, P. R. China. E-mail: zmsu@nenu.edu.cn*

[b] *School of Chemistry and Materials Science, Jiangsu Key Laboratory of Biofunctional Materials, Nanjing Normal University, Nanjing 210023, P. R. China. E-mail: liuj@njnu.edu.cn; yqlan@njnu.edu.cn*

[c] *School of Chemistry and Environmental Engineering, The Collaborative Innovation Center of Optical Materials and Chemistry, CUST, Changchun University of Science and Technology, Changchun 130028, P. R. China*

† Electronic supplementary information (ESI) available: Experimental methods and supporting figures and tables. CCDC 1855992–1855994. For ESI and crystallographic data in CIF or other electronic format see DOI: 10.1039/c8sc03471k

which has been surveyed extensively in different catalytic reaction types.[30–35] A lot of classic POM units or POM-based derivatives often exhibit favourable responses to specific catalytic reactions, where the relevant active sites and electron transfer of the catalytic reaction can be explained by their crystal structures.[36–40] However, the dissolvability of traditional POM clusters has been a major limiting factor for catalytic durability and needs to be primarily considered. So, the structural stability is the prerequisite for POM chemistry to be applied in any heterogeneous catalysis. As far as we know, high dimensional POM-containing inorganic architecture compared with the POM monomer usually shows good structural insolubility and an extended solar spectrum absorption range, which have been investigated in many photo-stimulated catalytic reactions such as water splitting, organic degradation, *etc.* In these reactions, the fast and reversible multi-electron transfer character of the POM subunit plays an extremely important role in promoting photocatalytic performance.[41–44] In this context, a POM-assembled inorganic complex is also believed to have advantages in the field of the heterogeneous photocatalytic CO_2RR. In particular, if the POM component within the structure can offer the CO_2 molecule sufficient electrons, then multi-electron oriented reductive products would be achievable.

Herein, we report two stable POM-containing inorganic compounds, $H\{[Na_2K_4Mn_4(PO_4)(H_2O)_4]\subset\{[Mo_6O_{12}(OH)_3(HPO_4)_3(PO_4)]_4[Mn_6(H_2O)_4]\}\cdot16H_2O$ (**NENU-605**) and $H\{[Na_6CoMn_3(PO_4)(H_2O)_4]\subset\{[Mo_6O_{12}(OH)_3(HPO_4)_3(PO_4)]_4[Co_{1.5}Mn_{4.5}]\}\cdot21H_2O$ (**NENU-606**), which have very similar host skeletons but different catalytically active species. It is noted that assembling $\{P_4Mo_6^V\}$ ($[Mo_6O_{12}(OH)_3(HPO_4)_3(PO_4)]^{6-}$) units with strong reducibility into the structures endows **NENU-605** and **NENU-606** with efficient heterogeneous photocatalytic CO_2-to-CH_4 reduction ability in water. To our knowledge, this is the first report of $\{P_4Mo_6^V\}$-based crystalline inorganic materials applied in the photocatalytic CO_2RR. Photocatalytic analysis revealed that the synergistic combination of strong reductive $\{P_4Mo_6^V\}$ units (donating electrons) and the first-row transition metal active centres (Mn^{II}/$Co^{II}Mn^{II}$) in **NENU-605** and **NENU-606** effectively boosts the necessary eight-electron reduction process for CH_4 evolution. Furthermore, the hetero-metallic active sites of **NENU-606** finally exhibited a higher CH_4 generation selectivity (85.5%) in the photocatalytic CO_2RR than those of **NENU-605** (76.6%). Besides, the coordination effect of alkali metal ions can also assist the accomplishment of the photocatalytic reaction by influencing the CO_2 adsorption ability of the title compounds. At the same time, the crystalline and heterogeneous nature of these stable inorganic POM-included compounds also provides some insight into the photocatalytic CO_2RR mechanism.

Results and discussion

NENU-605 and **NENU-606** were prepared by a hydrothermal synthesis method with a slight difference in the use of metal salts and organic templates, and they can be clearly distinguished by the colour and shape of the crystals (Fig. S1†). Single crystal X-ray diffraction analysis reveals that **NENU-605** and **NENU-606** crystallize in the same $I4_1/acd$ tetragonal space group and have very similar pure inorganic matrices composed of three kinds of independent Mn^{II}/Co^{II}–Mn^{II} ions, Na^+–K^+/Na^+ ions, $\{P_4Mo_6^V\}$ polyanions, phosphate anions and water molecules (Fig. S2†). The overall three-dimensional (3D) architecture of these two compounds is assembled with nesting subunits by using PO_4^{3-} and O^{2-} bridges. Such a nested substructure in **NENU-605** can be described as a three-shell assembly where the PO_4^{3-} group is the innermost shell (Fig. 1a). Four μ_2-O atoms of PO_4^{3-} connect with four six-coordinated Mn1 and four K1 atoms, and these Mn1 and K1 atoms establish two types of metal-based tetrahedrons respectively. The interpenetrating coupling of two tetrahedra forms a twisted hexahedron whose diagonal-linked vertexes are occupied by Mn1 or K1 atoms. Meanwhile, the top and bottom surfaces of this hexahedron are capped by two Na atoms to build the shuttle-shaped second shell (Fig. 1b). Through the $16PO_4^{3-}$ and $8O^{2-}$ groups, the second shell further communicates with the outer four Mn2 atoms and four $\{Mo_6^V\}$ rings. Each Mn2 atom is coordinated by five O atoms from four PO_4^{3-} anions and one O atom from the coordinated water molecule (Fig. S3†) and is surrounded by four $\{Mo_6^V\}$ rings made of six edge-sharing $\{Mo^VO_6\}$ octahedrons. It is noted that every $\{Mo_6^V\}$ ring supported by four PO_4^{3-} anions constitutes a strong reductive component, $P_4Mo_6^V$,[45–49] which includes six Mo^V atoms (Fig. S4†). Interestingly, these Mn2 atoms and $\{Mo_6^V\}$ rings can construct peripherally larger distorted hexahedrons in the same interpenetrating way as the second shell; the diagonal-linked vertexes are occupied by Mn2 atoms or $\{Mo_6^V\}$ rings that can be treated as the third shell (Fig. 1c). In such a way, a three-shell nested substructure is formed (Fig. 1d). To better further understand the evolution of this nested subunit, it has been simplified as a distorted hexahedral entity whose eight vertexes are taken up by Mn2 atoms and $\{Mo_6^V\}$ rings, as shown in Fig. 2a and b. These Mn2 atoms and $\{Mo_6^V\}$ rings serve as nodes to come into contact with the eight adjacent subunits in Mn2-to-Mn2 and $\{Mo_6^V\}$–Mn3–$\{Mo_6^V\}$ modes (Fig. 2c), which finally gives rise to the 3D inorganic structure of **NENU-605** (Fig. 2d). The linkage of Mn2-to-

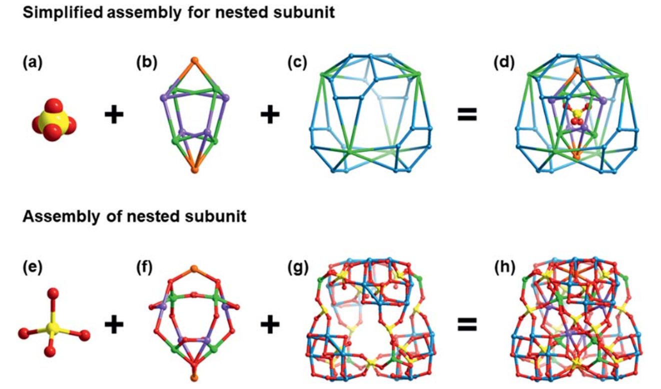

Fig. 1 Simplified (a–d) and real (e and h) three-shell nested subunit for **NENU-605**. (a, e) The innermost shell (central PO_4^{3-} group); (b, f) the shuttle-shaped second shell ($\{Na_2K_4Mn_4\}$); (c, g) the cage-like outermost shell ($Mn_4(\{P_4Mo_6\})_4$); (d, h) the overall three-shell nested substructure. Colour code: P yellow, O red, Na orange, K light purple, Mn green, and Mo light blue.

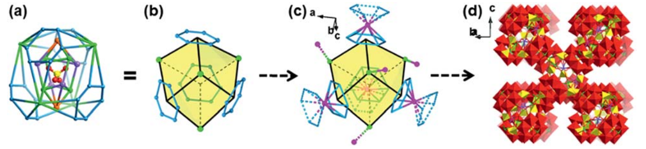

Fig. 2 Graphical growth of the 3D architecture of **NENU-605**: (a) simplified three-shell nested substructure; (b) further simplified nested substructure as a distorted hexahedral entity (Mn2, green; $\{Mo_6^V\}$ ring, light blue); (c) nested substructure with an 8-connected node in contact with the eight adjacent subunits (Mn2/Mn3, pink; $\{Mo_6^V\}$ ring, dashed light blue); (d) real 3D inorganic structure of **NENU-605**.

Mn2 is achieved by two μ_2-O atoms from two PO_4^{3-}, while every six-coordinated Mn3 atom is shared by two $\{Mo_6^V\}$ rings from two neighboring subunits (Fig. S5†). For **NENU-606**, the coordination environment of the Mn2 atom is crooked tetragonal pyramid structure consisting of five O atoms from four PO_4^{3-} groups (Fig. S6†); moreover the K1 atoms are fully replaced by Na atoms (Fig. S7†). The most important difference between these two compounds is that the original Mn atom sites in the lattice of **NENU-605** are partially substituted by Co atoms, and the doping ratio (1 : 3) of Co/Mn in **NENU-606** is determined by an Inductively Coupled Plasma Atomic Emission Spectrometer (ICP-AES). Besides, if the nested substructure and the Mn2/Mn3 atoms are regarded as 8-connected nodes and linkers, respectively, then the skeletons of **NENU-605** and **NENU-606** feature a unimodal topology with the Schläfli symbol of $4^{24}\cdot6^4$ (Fig. S8†).

The phase purity and thermal stability of **NENU-605** and **NENU-606** were demonstrated using well-matched powder X-ray diffraction (PXRD) patterns and thermogravimetric analysis, respectively (Fig. S9 and S10†). As shown in Fig. S9a and b,† these two compounds can also remain stable when being soaked in aqueous solutions at different pH values for several days, which indicated that their structures have strong acid and alkali resistance.[50] Besides, in order to confirm the heterogeneous catalytic nature, the structural stability of the title compounds was tested again under the conventional conditions of the photocatalytic CO_2RR. It is obvious that the PXRD patterns of all the treated crystals remain intact, indicating that no phase transition or structural collapse occurred. A broad UV-vis absorption range of 200–600 nm for **NENU-605** and **NENU-606** revealed that they indeed have better light-harvesting ability than a single POM cluster, whose absorption mainly focuses on the ultraviolet region (200–400 nm).[51–53] Based on this, the band gaps of 3.20 (**NENU-605**) and 2.57 eV (**NENU-606**) were evaluated by the Kubelka–Munk (KM) method (Fig. S11†), unveiling the potential for these two compounds to be used as semiconducting photocatalysts. At the same time, Mott–Schottky measurements at frequencies of 1000, 1500, and 2000 Hz were used to determine the LUMO positions of **NENU-605** and **NENU-606** such that the occurrence of the photocatalytic CO_2RR and relevant reductive products can be simply inferred (Fig. S12 and S13†). As we can see, the LUMO locations of compounds are more negative than the reduction potentials required for producing CO (−0.53 V *vs.* NHE) and CH_4 (−0.24 V *vs.* NHE), indicating that the electrons can be transferred to the CO_2 molecule for further reduction.

Taking the above features of **NENU-605** and **NENU-606** into consideration, the photocatalytic CO_2RR was conducted under a pure CO_2 (1.0 atm, 293 K) atmosphere in an aqueous solution with triethanolamine (TEOA) as a sacrificial agent ($TEOA/H_2O$ = 2 : 28 mL, pH ≈ 10.5). In addition, $[Ru(bpy)_3]Cl_2\cdot6H_2O$ (0.01 mmol) as an auxiliary photosensitizer (PS) was added into the reaction system for increased visible-light absorption.[54] Because of the matched LUMO positions between the PS and catalysts (Fig. S14 and S15†), photo-generated electrons were allowed to migrate from the PS to the catalysts. During the whole photoreduction process, gaseous CH_4 and CO were the main reaction products detected by gas chromatography, while trace amounts of HCOOH were produced in the aqueous solution as detected by ion chromatography. Moreover, no competitive H_2 was produced during the whole reaction (Fig. S16†). With the increasing irradiation time, the yields of CO and CH_4 increase simultaneously at different reaction rates (Fig. 3a and b); the amount of CH_4 for **NENU-605** reached up to 170 nmol (*i.e.*, 894.7 nmol g^{-1} h^{-1}) after 19 h. In contrast, the maximum production of CH_4 achieved for **NENU-606** was 402 nmol (*i.e.*, 1747.8 nmol g^{-1} h^{-1}) after 23 h (Fig. 3c). Moreover, they finally exhibit a very high selectivity (CH_4 over CO) of 76.6% (**NENU-605**) and 85.5% (**NENU-606**) (Fig. 3c). It is significant that this is the first report of heterogeneous POM-based catalysts applied in the photocatalytic CO_2RR that exhibited such a high selectivity towards CH_4, although the corresponding CH_4 outputs are still very low and need to be greatly improved. The CO amounts determined after the reaction were 267.0 nmol g^{-1} h^{-1} (**NENU-605**) and 295.7 nmol g^{-1} h^{-1} (**NENU-606**), and the relevant parameters including the TONs and TOFs of these

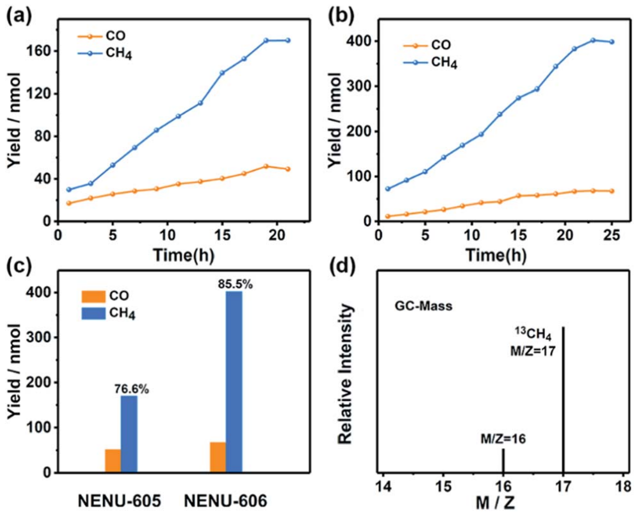

Fig. 3 Amounts of CH_4 and CO produced as a function of the time of visible-light irradiation using (a) **NENU-605** and (b) **NENU-606**; (c) total product yield and the selectivity of gaseous products in the photocatalytic CO_2RR; (d) the mass spectra of $^{13}CH_4$ recorded under a $^{13}CO_2$ atmosphere. The reaction with the catalyst (10 mg) in the $H_2O/TEOA$ (14 : 1 v/v, 30 mL) solution irradiated using a Xe lamp filtered to produce light in the range of 420–800 nm.

photocatalytic systems were summarized in Table S1.† **NENU-606** obviously has higher photocatalytic CH_4 selectivity than **NENU-605**, which can be further proved by their distinguishing transient photocurrent responses and electrochemical impedance spectra (Fig. S17†). The higher photocurrent response and smaller size of the Nyquist plot of **NENU-606** represented its better separation efficiency of photo-induced electron–hole pairs and faster interfacial charge transfer process compared to **NENU-605**. Such differences in the charge separation and the kinetics of charge transfer probably resulted from the different active sites in **NENU-605** (homometallic Mn^{II} ions) and **NENU-606** (heterometallic Mn^{II}/Co^{II} ions). Additionally, a series of reference experiments were carried out to explore the importance of each component in the photocatalytic reaction system, and the results are summed up in Table S1.† As we can see, in the absence of POM-based catalysts, TEOA, PSs, CO_2 or light illumination, no detectable products were observed in the reaction system. The photocatalytic durability of the compounds was tested to confirm their heterogeneous nature. From the time course plots of CH_4 evolution, the POM-containing catalysts maintain almost unchanged activities even after three cycles (Fig. S18†). The slight decline in the CH_4 evolution activity in subsequent runs is probably related to the small amount of mass loss of the samples used in the recovery process. Furthermore, there was no noticeable alteration in the PXRD patterns and IR and X-ray photoelectron (XPS) spectra obtained before and after the recycling experiments of the photocatalytic reaction that evidenced the structural robustness of **NENU-605** and **NENU-606** again (Fig. S9c, d, S19, S20 and S21†).

To exclude the influence of possible active component decomposition on the photocatalytic activity, the reaction solution was filtrated after irradiating 11 hours and then the filtrate was detected. The fact that the generation of CH_4 and CO would stop if the catalysts were removed from the reaction system clearly suggests that the photocatalytic activity comes from the catalysts themselves (Fig. S22†). Meanwhile, only trace amounts (**NENU-605**, 0.67%; **NENU-606**, 0.81%) of metal residue in the filtrate after the photocatalytic reaction were detected by ICP-AES. All these results pointed out that both **NENU-605** and **NENU-606** possess good photocatalytic durability towards the CO_2RR under visible-light irradiation. To further validate the source of the produced CO and CH_4, an isotope experiment using $^{13}CO_2$ as the substrate was performed, and then the associated products were analysed by gas chromatography and mass spectrometry.[55] As shown in Fig. S23† and 3d, the peaks at $m/z = 29$ and $m/z = 17$ were assigned to ^{13}CO and $^{13}CH_4$, respectively, providing solid proof that **NENU-605** and **NENU-606** are indeed active and capable of selectively converting CO_2 to CH_4 under visible-light irradiation.

To disclose the origin and difference of the photocatalytic performances of **NENU-605** and **NENU-606** in the CO_2RR, the role of the $\{Mn[Mo_6O_{12}(OH)_3(HPO_4)_3(PO_4)]_2\}$ (abbr.$\{Mn(P_4Mo_6)_2\}$) cluster (**NENU-607**) (Fig. S24–26†) was mainly considered in our system. **NENU-607** is a dimer, with one $\{Mn^{II}\}$ atom sandwiched between two $\{P_4Mo_6\}$ units, displaying a similar connection mode to that of **NENU-605** and **NENU-606**. When **NENU-607** was synthesized and used as a catalyst applied under identical conditions of the photocatalytic reaction, only a small amount of CO (47 nmol) and CH_4 (70 nmol) were detected, which demonstrated that the light-induced CO_2 reduction process more likely occurred on the active Mn^{II} ions (**NENU-605**) or Mn^{II}/Co^{II} ions (**NENU-606**). The strongly reductive $P_4Mo_6^V$ cluster including six Mo^V atoms in the case of redox reactions can theoretically offer multiple electrons for the CO_2RR. Because each Lewis acid metal active site in title compounds is surrounded by four $P_4Mo_6^V$ units, the achieved photo-stimulated CO_2-to-CH_4 conversion seems to be understandable. As for the higher CH_4 selectivity of **NENU-606** than **NENU-605**, we speculated that the interaction between hetero-metallic Mn^{II}/Co^{II} ions was more beneficial than that between homometallic Mn^{II} ions in terms of adsorption and activation of CO_2 molecules. Besides, the reaction medium was also found to be an important factor in influencing the catalytic result. When the aqueous solution was replaced by dry MeCN (entry 9, Table S1†), no noticeable reduction products can be detected in the photocatalytic system. Additionally, the generation of reduction products relies on the participation of H_2O as the solvent, as demonstrated in Fig. S27.† Moreover, the further increase of reduction products is also related to the increased amount of H_2O. All the above cases have suggested the importance of H_2O as the proton donor for the CO_2-to-CH_4 reduction reaction.

Based on the analysis of related experimental results, a speculative reaction mechanism with respect to the photocatalytic CO_2-to-CH_4 conversion using these two crystalline POM-containing compounds, as well as possible photo-generated electron transport pathways, was proposed (Fig. 4). First, the photosensitizer in the system absorbs sunlight to generate photo-excited electrons from the HOMO and then transports them to the catalyst through the matched LUMO positions; TEOA as the sacrificial reagent consumes the electron holes produced in the valence band. Second, strongly reductive $\{P_4Mo_6^V\}$ units enrich and offer electrons to the active metal centre under the stimulation of the photo-induced redox reaction. Third, the adsorbed CO_2 molecule obtains electrons from the active metal sites, with the assistance of H_2O as a proton donor, eventually undergoing the multi-electron transfer process of CO_2-to-CH_4 reduction. In addition, because the low

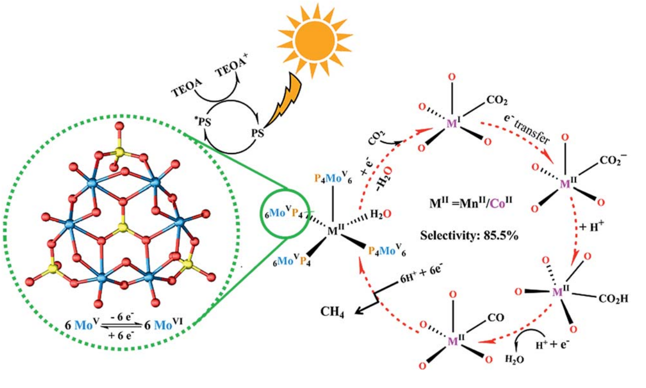

Fig. 4 Proposed mechanism for the photocatalytic reduction of CO_2 to CH_4 using **NENU-605** and **NENU-606**.

local concentration of CO_2 around the typical catalysts can make the reaction suffer from slow kinetics,[56,57] the coordination of alkali metal cations in **NENU-605** and **NENU-606** architectures is helpful to effectively physically adsorb CO_2 molecules through non-covalent interactions,[58,59] which could lower the overpotential and Gibbs free energy ΔG of the chemical reduction of CO_2.[60–62]

Conclusions

In summary, this is the first report of inorganic POM-containing crystalline materials as heterogeneous catalysts applied in the photocatalytic CO_2RR, and significant CO_2-to-CH_4 conversion in the aqueous phase is realized. Both **NENU-605** and **NENU-606** have almost identical 3D host structures composed of three-shell nested substructures, which were further composed of $\{P_4Mo_6\}$ clusters, first-row transition metals and alkali metals. Because of the strong reducibility and electron-enrichment of the $\{P_4Mo_6\}$ unit, sufficient electrons can be transported to active metal sites under the effect of the photo-stimulated redox reaction for the activation and reduction of CO_2 molecules. In virtue of the synergistic coupling of structural components, these compounds finally exhibit high photocatalytic CH_4 selectivity (76.6%, **NENU-605**; 85.5%, **NENU-606**). Especially for **NENU-606** with hetero-metallic active sites, the interaction between Mn^{II} and Co^{II} ions is found to be more efficient for the photocatalytic CO_2RR than that between the homo-metallic Mn^{II} ions in **NENU-605**. Notably, the introduction of the $\{P_4Mo_6\}$ building block not only endows **NENU-605** and **NENU-606** with favorable structural rigidity, but also, indeed, facilitates the accomplishment of the eight-electron transfer process of CH_4 formation by delivering sufficient electrons. We anticipate that such a feasible strategy, embedding strongly reductive components into the visible-light sensitized catalyst architecture, could inspire more enthusiasm to construct stable inorganic networks for the effective reduction of CO_2 to other high-valued hydrocarbons and further enhance their photocatalytic activity.

Conflicts of interest

There are no conflicts to declare.

Acknowledgements

This work was financially supported by NSFC (No. 21622104, 21471080, 21701085 and SBK2017040708), the NSF of Jiangsu Province of China (No. BK20171032), the Natural Science Research of Jiangsu Higher Education Institutions of China (No. 17KJB150025), Priority Academic Program Development of Jiangsu Higher Education Institutions and the Foundation of Jiangsu Collaborative Innovation Center of Biomedical Functional Materials.

Notes and references

1 C. Steinlechner and H. Junge, *Angew. Chem., Int. Ed.*, 2018, **57**, 44–45.
2 T. Sakakura, J.-C. Choi and H. Yasuda, *Chem. Rev.*, 2007, **107**, 2365–2387.
3 T. Inoue, A. Fujishima, S. Konishi and K. Honda, *Nature*, 1979, **277**, 637–638.
4 A. Rubino, *Nat. Energy*, 2018, **3**, 255–256.
5 X. Li, J. Wen, J. Low, Y. Fang and J. Yu, *Sci. China Mater.*, 2014, **57**, 70–100.
6 H. Rao, L. C. Schmidt, J. Bonin and M. Robert, *Nature*, 2017, **548**, 74–77.
7 X. Liu, S. Inagaki and J. Gong, *Angew. Chem., Int. Ed.*, 2016, **55**, 14924–14950.
8 X. Chang, T. Wang and J. Gong, *Energy Environ. Sci.*, 2016, **9**, 2177–2196.
9 K. Li, B. Peng and T. Peng, *ACS Catal.*, 2016, **6**, 7485–7527.
10 L. Zeng, X. Guo, C. He and C. Duan, *ACS Catal.*, 2016, **6**, 7935–7947.
11 Y. Fu, D. Sun, Y. Chen, R. Huang, Z. Ding, X. Fu and Z. Li, *Angew. Chem., Int. Ed.*, 2012, **51**, 3364–3367.
12 S. Wang, W. Yao, J. Lin, Z. Ding and X. Wang, *Angew. Chem.*, 2014, **126**, 1052–1056.
13 H. Zhang, J. Wei, J. Dong, G. Liu, L. Shi, P. An, G. Zhao, J. Kong, X. Wang, X. Meng, J. Zhang and J. Ye, *Angew. Chem.*, 2016, **128**, 14522–14526.
14 C. Wang, Z. Xie, K. E. deKrafft and W. Lin, *J. Am. Chem. Soc.*, 2011, **133**, 13445–13454.
15 Y. Wang, N.-Y. Huang, J.-Q. Shen, P.-Q. Liao, X.-M. Chen and J.-P. Zhang, *J. Am. Chem. Soc.*, 2018, **140**, 38–41.
16 H.-Q. Xu, J. Hu, D. Wang, Z. Li, Q. Zhang, Y. Luo, S.-H. Yu and H.-L. Jiang, *J. Am. Chem. Soc.*, 2015, **137**, 13440–13443.
17 D. Wang, R. Huang, W. Liu, D. Sun and Z. Li, *ACS Catal.*, 2014, **4**, 4254–4260.
18 W. Min, C. Lingjing, L. Tai-Chu and R. Marc, *Angew. Chem., Int. Ed.*, 2018, **57**, 7769–7773.
19 R. Kuriki, M. Yamamoto, K. Higuchi, Y. Yamamoto, M. Akatsuka, D. Lu, S. Yagi, T. Yoshida, O. Ishitani and K. Maeda, *Angew. Chem.*, 2017, **129**, 4945–4949.
20 R. Kuriki, H. Matsunaga, T. Nakashima, K. Wada, A. Yamakata, O. Ishitani and K. Maeda, *J. Am. Chem. Soc.*, 2016, **138**, 5159–5170.
21 W. Tu, Y. Zhou and Z. Zou, *Adv. Mater.*, 2014, **26**, 4607–4626.
22 S. N. Habisreutinger, L. Schmidt-Mende and J. K. Stolarczyk, *Angew. Chem., Int. Ed.*, 2013, **52**, 7372–7408.
23 Y. Fang and X. Wang, *Chem. Commun.*, 2018, **54**, 5674–5687.
24 G. Chao, M. Qiangqiang, Z. Kun, Y. Huajie, W. Dawei, G. Jun, Z. Shenlong, C. Lin, H. Meng, L. Qunxiang, Z. Huijun, H. Xingjiu, G. Yan and T. Zhiyong, *Adv. Mater.*, 2016, **28**, 6485–6490.
25 R. Long, Y. Li, Y. Liu, S. Chen, X. Zheng, C. Gao, C. He, N. Chen, Z. Qi, L. Song, J. Jiang, J. Zhu and Y. Xiong, *J. Am. Chem. Soc.*, 2017, **139**, 4486–4492.
26 C. Gao, S. Chen, Y. Wang, J. Wang, X. Zheng, J. Zhu, L. Song, W. Zhang and Y. Xiong, *Adv. Mater.*, 2018, **30**, 1704624–1704632.
27 S. Yongfu, W. Ju, L. Xiaodong, S. Wen, L. Peiquan, J. Xingchen, G. Shan, L. Liang, X. Jiaqi, Y. Wensheng, W. Chengming and X. Yi, *Angew. Chem.*, 2018, **130**, 8855–8859.

28 S. Wang, B. Y. Guan, Y. Lu and X. W. D. Lou, *J. Am. Chem. Soc.*, 2017, **139**, 17305–17308.

29 R. Kuriki, T. Ichibha, K. Hongo, D. Lu, R. Maezono, H. Kageyama, O. Ishitani, K. Oka and K. Maeda, *J. Am. Chem. Soc.*, 2018, **140**, 6648–6655.

30 J. Ettedgui, Y. Diskin-Posner, L. Weiner and R. Neumann, *J. Am. Chem. Soc.*, 2011, **133**, 188–190.

31 J. Dong, J. Hu, Y. Chi, Z. Lin, B. Zou, S. Yang, C. L. Hill and C. Hu, *Angew. Chem.*, 2017, **129**, 4544–4548.

32 S. Mukhopadhyay, J. Debgupta, C. Singh, A. Kar and S. K. Das, *Angew. Chem.*, 2018, **130**, 1936–1941.

33 A. Proust, B. Matt, R. Villanneau, G. Guillemot, P. Gouzerh and G. Izzet, *Chem. Soc. Rev.*, 2012, **41**, 7605–7622.

34 P. Yang and U. Kortz, *Acc. Chem. Res.*, 2018, **51**, 1599–1608.

35 M. Zhao, X.-W. Zhang and C.-D. Wu, *ACS Catal.*, 2017, **7**, 6573–6580.

36 L.-X. Cai, S.-C. Li, D.-N. Yan, L.-P. Zhou, F. Guo and Q.-F. Sun, *J. Am. Chem. Soc.*, 2018, **140**, 4869–4876.

37 W. Guo, H. Lv, Z. Chen, K. P. Sullivan, S. M. Lauinger, Y. Chi, J. M. Sumliner, T. Lian and C. L. Hill, *J. Mater. Chem. A*, 2016, **4**, 5952–5957.

38 T. Ishizuka, S. Ohkawa, H. Ochiai, M. Hashimoto, K. Ohkubo, H. Kotani, M. Sadakane, S. Fukuzumi and T. Kojima, *Green Chem.*, 2018, **20**, 1975–1980.

39 B. B. Sarma, I. Efremenko and R. Neumann, *J. Am. Chem. Soc.*, 2015, **137**, 5916–5922.

40 H. Shi, Y. Yu, Y. Zhang, X. Feng, X. Zhao, H. Tan, S. U. Khan, Y. Li and E. Wang, *Appl. Catal., B*, 2018, **221**, 280–289.

41 S. Li, S. Liu, S. Liu, Y. Liu, Q. Tang, Z. Shi, S. Ouyang and J. Ye, *J. Am. Chem. Soc.*, 2012, **134**, 19716–19721.

42 M. Natali, I. Bazzan, S. Goberna-Ferrón, R. Al-Oweini, M. Ibrahim, B. Bassil, H. Dau, F. Scandola, J. Galán-Mascarós and U. Kortz, *Green Chem.*, 2017, **19**, 2416–2426.

43 A. Rubinstein, P. Jiménez-Lozanao, J. J. Carbó, J. M. Poblet and R. Neumann, *J. Am. Chem. Soc.*, 2014, **136**, 10941–10948.

44 K. Suzuki, F. Tang, Y. Kikukawa, K. Yamaguchi and N. Mizuno, *Angew. Chem., Int. Ed.*, 2014, **53**, 5356–5360.

45 Y. Dong, Z. Dong, Z. Zhang, Y. Liu, W. Cheng, H. Miao, X. He and Y. Xu, *ACS Appl. Mater. Interfaces*, 2017, **9**, 22088–22092.

46 D.-Y. Du, J.-S. Qin, Y.-G. Li, S.-L. Li, Y.-Q. Lan, X.-L. Wang, K.-Z. Shao, Z.-M. Su and E.-B. Wang, *Chem. Commun.*, 2011, **47**, 2832–2834.

47 K. Gong, W. Wang, J. Yan and Z. Han, *J. Mater. Chem. A*, 2015, **3**, 6019–6027.

48 Z. Han, X. Xin, R. Zheng and H. Yu, *Dalton Trans.*, 2018, **47**, 3356–3365.

49 D.-Y. Du, J.-S. Qin, T.-T. Wang, S.-L. Li, Z.-M. Su, K.-Z. Shao, Y.-Q. Lan, X.-L. Wang and E.-B. Wang, *Chem. Sci.*, 2012, **3**, 705–710.

50 E.-X. Chen, M. Qiu, Y.-F. Zhang, Y.-S. Zhu, L.-Y. Liu, Y.-Y. Sun, X. Bu, J. Zhang and Q. Lin, *Adv. Mater.*, 2018, **30**, 1704388–1704395.

51 E. Haviv, L. J. W. Shimon and R. Neumann, *Chem.–Eur. J.*, 2017, **23**, 92–95.

52 C. Li, K. Suzuki, N. Mizuno and K. Yamaguchi, *Chem. Commun.*, 2018, **54**, 7127–7130.

53 J. J. Walsh, A. M. Bond, R. J. Forster and T. E. Keyes, *Coord. Chem. Rev.*, 2016, **306**, 217–234.

54 T. Ouyang, H.-H. Huang, J.-W. Wang, D.-C. Zhong and T.-B. Lu, *Angew. Chem., Int. Ed.*, 2017, **56**, 738–743.

55 J. Zhao, Q. Wang, C. Sun, T. Zheng, L. Yan, M. Li, K. Shao, X. Wang and Z. Su, *J. Mater. Chem. A*, 2017, **5**, 12498–12505.

56 S. Back, M. S. Yeom and Y. Jung, *ACS Catal.*, 2015, **5**, 5089–5096.

57 Q. Lu, J. Rosen, Y. Zhou, G. S. Hutchings, Y. C. Kimmel, J. G. Chen and F. Jiao, *Nat. Commun.*, 2014, **5**, 3242–3247.

58 Y. Chen, C. W. Li and M. W. Kanan, *J. Am. Chem. Soc.*, 2012, **134**, 19969–19972.

59 A. S. Varela, M. Kroschel, T. Reier and P. Strasser, *Catal. Today*, 2016, **260**, 8–13.

60 M. Liu, Y. Pang, B. Zhang, P. De Luna, O. Voznyy, J. Xu, X. Zheng, C. T. Dinh, F. Fan, C. Cao, F. P. de Arquer, T. S. Safaei, A. Mepham, A. Klinkova, E. Kumacheva, T. Filleter, D. Sinton, S. O. Kelley and E. H. Sargent, *Nature*, 2016, **537**, 382–386.

61 J. Resasco, L. D. Chen, E. Clark, C. Tsai, C. Hahn, T. F. Jaramillo, K. Chan and A. T. Bell, *J. Am. Chem. Soc.*, 2017, **139**, 11277–11287.

62 M. R. Singh, Y. Kwon, Y. Lum, J. W. Ager III and A. T. Bell, *J. Am. Chem. Soc.*, 2016, **138**, 13006–13012.